THE ASTROPHYSICAL JOURNAL, 403:175–182, 1993 January 20

DENSE CORES IN L1204/S140: STAR FORMATION AND VELOCITY SHIFTS

M. TAFALLA,[1,2] R. BACHILLER,[2] AND J. MARTÍN-PINTADO[2]
Received 1992 March 25; accepted 1992 July 28

ABSTRACT

We observe the dense gas in the L1204/S140 molecular complex using CS($J = 1$–0) and NH_3. The large-scale CS($J = 1$–0) maps show that L1204 is formed by three filamentary clouds, each being fragmented into cores of a few hundred solar masses and surrounded by low-level emission. The most prominent core is associated with S140, a well-known high-mass star-forming region. The star-forming activity, however, is not restricted to the vicinity of S140, but extends throughout the complex; very red *IRAS* sources lie close to most of the cores and molecular outflows have been detected in half of them. The ammonia observations reveal velocity shifts of $\sim$0.5–0.8 km s^{-1} in the dense gas inside the cores with embedded stars. These velocity shifts, although small, are systematic and tend to divide the cores into two velocity regimes with little overlap. Fast rotation of the cores or the interaction between the bipolar outflows and the dense gas (or a combination of both) are the most likely causes for these velocity shifts.

Subject headings: H II regions — ISM: individual (L1204) — ISM: jets and outflows — ISM: kinematics and dynamics — ISM: molecules

1. INTRODUCTION

S140 is the H II region seen as the bow-shaped, bright edge of the L1204 dark cloud. In the proximity of S140 lies a cluster of infrared objects (Blair & Vanden Bout 1974), probably composed of embedded main-sequence stars of late O or early B type (Lester et al. 1986; Evans et al. 1989). The vicinity of this cluster, with its strong molecular emission, has been the focus of numerous studies; the CO profiles present high-velocity wings (Blair et al. 1978) that indicate the existence of a bipolar outflow, and high-density tracers have probed gas at densities of several times 10^5 cm^{-3} (Snell et al. 1984). Most of the studies of L1204, however, have been limited to the immediate vicinity of the infrared cluster and very little is known about the overall properties of the cloud. Only recently have large-scale maps been available. The ^{13}CO($J = 1$–0) maps of Sugitani & Fukui (1987) show that L1204 extends over $0.^{\circ}5 \times 1^{\circ}$ and contains several velocity components. These observations, however, are insensitive to the density structure of the cloud, which should be studied with transitions from high dipole moment molecules.

In this paper we present the results of CS and NH_3 mapping of L1204, as well as a search in CO for molecular outflows at selected positions. The technical details of the observations are given in § 2. We discuss the large-scale CS($J = 1$–0) emission in § 3, where we also study the star-forming activity in the cloud by using data from the *IRAS* survey and the results from the search for molecular outflows in CO($J = 2$–1). In § 4 we describe high-resolution ammonia mapping of the cores with particular attention to the kinematics of the dense gas. The origin of the kinematics and the relation between CS and NH_3 emissions are discussed in § 5.

2. OBSERVATIONS

The CS($J = 1$–0) observations were carried out with the 14 m telescope of the Centro Astronómico de Yebes, near Guadalajara (Spain). The receiver was an uncooled Schottky diode mixer with a noise temperature of $\sim$210 K (DSB). The spectrometer was a filter bank with 256 channels of 50 kHz width, which provided a spectral resolution of $\sim$0.31 km s^{-1} at 49 GHz. The observations were made in frequency switching mode. Measurements on Jupiter and the Moon were used to determine a half-power beam width (HPBW) of 2′ and a coupling coefficient for extended sources of $\sim$0.43. The data were calibrated by the chopper-wheel method. The calibration and pointing were tested by frequent observations of the central position of S140. The data are expressed in units of T_R^* in the sense of Kutner & Ulich (1981).

The NH_3 (1, 1) and (2, 2) observations were carried out with the 100 m telescope at Effelsberg (F.R.G.) in 1988 November. The receiver was a maser giving typical noise temperatures of 60 K (including the atmosphere). The spectrometer was an autocorrelator which was split into two 6.25 MHz bands of 512 channels each, centered on the (1, 1) and (2, 2) frequencies. This configuration gives a spectral resolution of 0.15 km s^{-1}. The antenna beam size at 23.7 GHz was $\sim$40″. The observations were made in position switching mode, and pointing was frequently checked during each session by cross scans on continuum sources. Calibration was achieved by observing NGC 7027, for which we assumed a main beam brightness temperature of 8.3 K at 23.7 GHz. Intensities are given in units of main beam Rayleigh-Jeans brightness temperature.

The CO($J = 2$–1) observations were carried out with the IRAM 30 m radio telescope at Pico Veleta (near Granada, Spain) in 1990 April. We used an SIS receiver with SSB noise temperature of $\sim$250 K. At 230.5 GHz, the HPBW was 12″, and the main beam efficiency was 0.45. Pointing was checked by observing nearby continuum sources and was found to be accurate within 3″. The spectrometer was a filter bank of 512×1 MHz channels providing a spectral resolution of 1.3 km s^{-1}. Our main goal was to search for high-velocity CO(2–1) emission around the positions of *IRAS* sources in the L1204/S140 complex. As flat baselines were essential to detect eventual weak wings, we made the observations in position switching mode with the reference OFF position relatively close to the ON source positions (typically at distances of $\sim$5′).

[1] Astronomy Department and Radio Astronomy Laboratory, University of California at Berkeley, 601 Campbell Hall, Berkeley, CA 94720.
[2] Centro Astronómico de Yebes (IGN). Apartado 148, E-19080, Guadalajara, Spain.

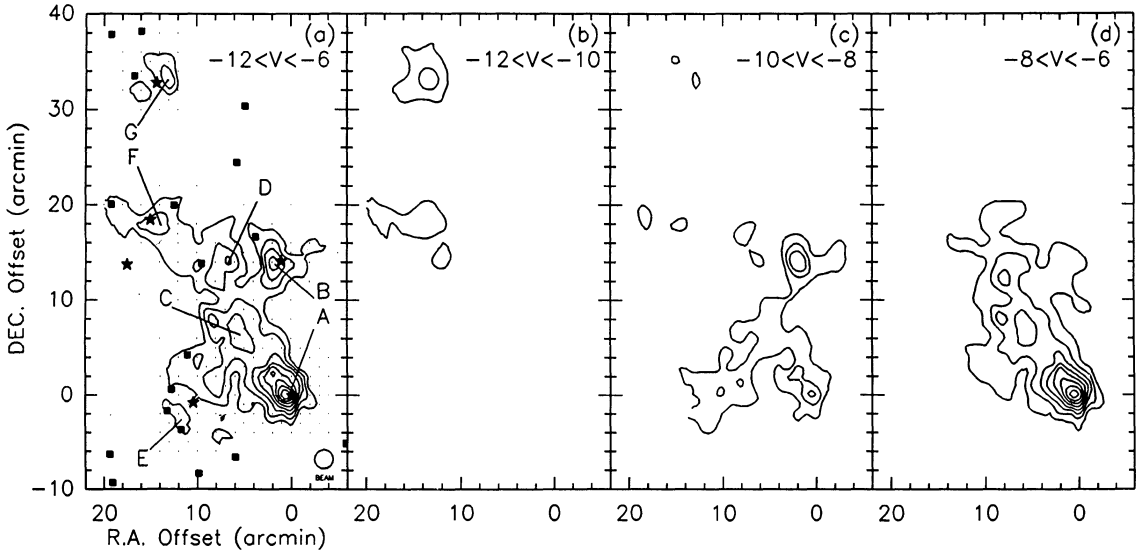

FIG. 1.—CS(1–0) maps of the L1204/S140 complex. The (0, 0) position is on S140-IRS at $\alpha(1950) = 22^h17^m42^s$, $\delta(1950) = 63°03'45''$. (*a*) Integrated emission in the velocity range −12 to −6 km s^{-1}. Contour levels are 1.2, 2.1, 3.0, ... K km s^{-1}. The *IRAS* sources within the region are represented by filled squares and selected *IRAS* sources (see text) are represented by filled stars. (*b*) Map of integrated antenna temperature in the velocity range −12 to −10 km s^{-1}. Contours are at 0.7, 1.4, ... K km s^{-1}. (*c*) Same as (*b*) in the velocity range −10 to −8 km s^{-1}. (*d*) Same as (*b*) in the velocity range −8 to −6 km s^{-1}.

This observing procedure resulted in spectra which may be contaminated at ambient velocities. Hence, the CO emission at ambient velocities will not be further discussed in this paper, and we will deal only with the emission at high velocities.

3. RESULTS FROM CS AND CO OBSERVATIONS

3.1. CS *Cores and Kinematics*

The CS(1–0) integrated intensity map of Figure 1*a* shows that L1204 is highly fragmented and consists of at least seven cores interconnected by low-level emission. The most prominent core, A, contains the infrared cluster S140-IRS. Most of the other cores are also associated with young stellar objects (YSOs) (§ 3.3), indicating that star-forming activity extends throughout L1204.

L1204 has a rich velocity structure, and the maps in Figures 1*b*, 1*c*, and 1*d* show that the cores are distributed in three elongated clouds with different velocities. These CS(1–0) maps are in good agreement with the ^{13}CO(1–0) maps of Sugitani & Fukui (1987, hereafter SF), with the CS emission more concentrated, as it only traces the denser gas. In both ^{13}CO and CS maps, the most prominent cloud appears between −8 and −6 km s^{-1} (Fig. 1*d* for CS) and will be referred as L1204-1. It extends southwest-northeast and has a head-tail structure surrounded by low-level emission. The head is centered on S140-IRS, and the tail is formed by cores C and D. L1204-1 has an additional condensation in the vicinity of core F. It does not appear in the CS maps, but an average of the spectra over that region shows two components, one of them at $V_{LSR} = -7.4$ km s^{-1}, characteristic of L1204-1. This core (F′) can be seen in the higher resolution ammonia maps of Figure 4, below, as a secondary peak northwest of F. All the cores in L1204-1 have similar velocities, around −7 km s^{-1} (see Table 1), and the cloud does not present any systematic velocity gradient. The second cloud of L1204 (L1204-2) appears in the velocity range −10 to −8 km s^{-1}. Figure 1*c* shows that L1204-2 is also elongated, extending from core E to core B through core C, and seems to be perpendicular to L1204-1. The emission from core A in this velocity range is due to the contribution from the strong wings of spectra with $V_{LSR} = -7.2$ km s^{-1} and not from lines centered between −10 and −8 km s^{-1}; no gas from the core A region seems to belong to L1204-2. Cores B and E have similar LSR velocities, −8.6 and −8.8 km s^{-1}, indicating the absence of velocity gradients along L1204-2. Finally, the L1204-3 cloud appears in the −12 to −10 km s^{-1} map (Fig. 1*b*) and contains cores F and G. They have similar velocities (−10.3 and −10.8 km s^{-1}), and although there is no evidence for their connection in the CS(1–0) map, the ^{13}CO data from SF show low-level emission extending from one core to the other. In core G the CS(1–0) spectra present a velocity shift of

TABLE 1

CORE PARAMETERS

Core	Offset[a] ($\Delta\alpha$, $\Delta\delta$)	T_R^* (K)	$\int T_R^* dV$ (K km s^{-1})	ΔV (km s^{-1})	V_{LSR} (K km s^{-1})	M_{vir} ($M_\odot$)	M_{min}^{LVG} ($M_\odot$)
A	(0, 0)	3.2	8.7	2.5	−7.2	880	1130
B	(2, 14)	1.8	4.0	2.0	−8.6	540	320
C	(6, 8)	1.4	4.3	3.0	−6.9	970	580
D	(8, 12)	1.3	3.2	2.2	−6.7	850	450
E	(12, −2)	1.2	1.4	1.1	−8.8	290	250
F	(14, 20)	0.9	0.9	1.0	−10.3	400	300
G	(14, 34)	1.2	1.6	1.3	−10.8	530	200

[a] Offset in arcminutes with respect to the central position of the maps in Fig. 1.

~ 0.8 km s^{-1} in the north-south direction. These shifts are common in the ammonia lines from most of the cores and are discussed in § 4.2.

3.2. *Masses*

We have estimated the masses of the dense cores by applying the virial theorem. Assuming equilibrium between self-gravity and turbulent pressure, the virial mass of an homogeneous spherical system is given by (see, e.g., MacLaren, Richardson, & Wolfendale 1988)

$$M_{\rm vir} = 210\left(\frac{R}{1\ \rm pc}\right)\left(\frac{\Delta V}{1\ \rm km\ s^{-1}}\right)^2 M_\odot\ .$$

In order to estimate the core radii (R), we have divided the cloud into seven regions, each associated by its kinematics to one of the cores. A distance of 910 pc to the L1204 complex was assumed, based on the spectroscopic parallax to the exciting star of S140 given by Crampton & Fisher (1974). The resulting virial estimates appear in Table 1; each core seems to contain a few hundred solar masses, and the sum of all the masses gives an estimate of $4.5 \times 10^3\ M_\odot$ for the total mass of the complex.

Since internal motions (see § 4.2) and boundaries smeared by extended low-level emission may lead to systematically overestimated virial masses, it is important to obtain a mass lower limit. We have done so by converting the observed CS intensities into minimum column densities. We have solved the equations of radiative transfer using the large velocity gradient (LVG) approximation (e.g, Castor 1970) that, for an homogeneous cloud, only requires as input parameters the particle density (n), the CS column density over the line width [N(CS)/ΔV], and the kinetic temperature (T_K) (Scoville & Solomon 1974). As Figure 2*a* shows, for a fixed kinetic temperature, any contour of observed intensity T_R always stays to the right of a certain value of $N(\rm CS)/\Delta V$. By estimating ΔV from a Gaussian fit to the spectrum, a lower limit to N(CS) is obtained. Figure 2*b* gives the minimum $N(\rm CS)/\Delta V$ as a function of T_R for several kinetic temperatures, showing that for the T_R values in L1204 (~ 1 K), the minimum CS column density is rather insensitive to the kinetic temperature. We have assumed a value of 20 K, as suggested by our ammonia data (§ 4.1). In order to calculate the mass lower limit, the CS column density has to be converted into H_2 column density, and the value of the CS abundance is the largest uncertainty in the mass estimate. We have used 1.6×10^{-9}, a compromise among the measured values for TMC1, Orion, and Sgr-B2 (2×10^{-9}, 8.3×10^{-10}, and 3×10^{-9}, respectively; Leung, Herbst, & Huebner 1984). The calculated minimum masses for the different cores in the L1204 complex are presented in Table 1; again, the cores are estimated to have a few hundred solar masses each, and the total (minimum) mass is $\sim 3 \times 10^3\ M_\odot$, similar to the virial result.

Because of all the uncertainties involved in the two mass estimates, their agreement cannot be used to obtain any firm conclusion on the equilibrium state of the cores or on the CS abundance. It seems to indicate, however, that the total amount of dense gas is $3\text{–}5 \times 10^3\ M_\odot$, similar to the $10^4\ M_\odot$ given by SF for the less dense gas traced by ^{13}CO.

3.3. *Star Formation in the* CS *Cores: IRAS Point Sources and High-Velocity* CO

Most of the dense cores seem to be associated with infrared objects. This is shown in Figure 1*a*, where we have represented the positions of all the *IRAS* point sources in the vicinity of L1204 (*IRAS* Point Source Catalog 1988). From a total of 23 sources, only six were detected in at least three *IRAS* bands; they are represented by filled stars in Figure 1*a*, and their fluxes are listed in Table 2. Five of these six sources lie in the vicinity of dense cores, and they have infrared energy distributions with most of the flux coming from the longest wavelengths. This type of distribution seems to be characteristic of YSOs, still deeply embedded in their forming core (Lada 1987) and, in fact, the *IRAS* source associated with core A is S140-IRS, a well-known cluster of young stars (Blair & Vanden Bout 1974).

In order to decide whether the other five selected *IRAS* sources are also YSOs, we have observed them in CO(2–1) searching for high-velocity emission, a signature of molecular outflow. Three of them (associated with cores B, F, and G) show definite evidence for high-velocity gas, confirming their true nature as YSOs. We present their CO(2–1) spectra in Figure 3. IRAS 22178+6317 (in core B) was previously known to have a bipolar outflow (Fukui et al. 1986), and our spectrum shows high-velocity gas with $\Delta V_{zi} \approx 40$ km s^{-1} (full width at

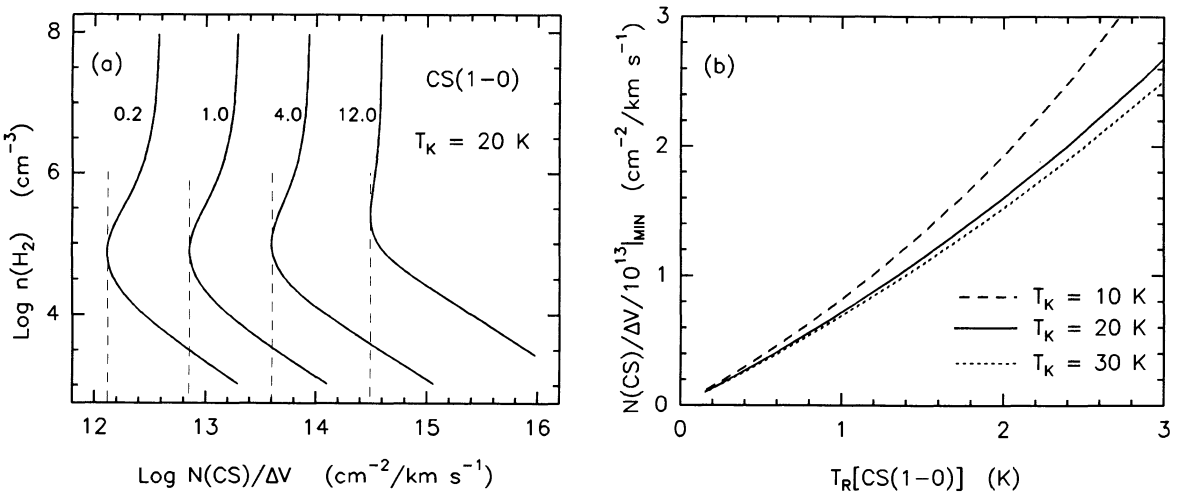

FIG. 2.—Results from LVG radiative transfer calculations. (*a*) Curves of constant CS(1–0) antenna temperature (T_R) for a model with $T_K = 20$ K. The dashed vertical lines indicate the minimum $N(\rm CS)/\Delta V$ for each T_R. (*b*) Minimum $N(\rm CS)/\Delta V$ (in units of 10^{13} cm^{-3}/km s^{-1}) as a function of T_R for different kinetic temperatures.

TABLE 2

SELECTED *IRAS* OBJECTS

IRAS Number	Core	$S_{12\,\mu m}$ (Jy)	$S_{25\,\mu m}$ (Jy)	$S_{60\,\mu m}$ (Jy)	$S_{100\,\mu m}$ (Jy)	L_{IRAS} ($L_\odot$)	CO Flow?
22176+6303	A	308	1540	11232	13463	1.5×10^4	Y
22178+6317	B	5.2	14.4	61.6	213	130	Y
22192+6302	E	0.64	0.96	56.3	<259	<80 (>20)	N
22198+6336	G	<0.25	23.3	187	415	250	Y
22199+6322	F	0.80	3.82	20.2	<55.2	<35 (>20)	Y
22202+6317	?	0.47	1.61	14.2	<55.2	<25 (>10)	N

zero intensity). The other sources with outflows are IRAS 22199+6322 (in core F), with $\Delta V_{zi} \approx 35$ km s^{-1}, mostly blue gas, and IRAS 22198+6336 (in core G), with $\Delta V_{zi} \approx 30$ km s^{-1}. These two outflows have been independently detected by Fukui (1989). On the other hand, we have not found any evidence for high-velocity gas toward IRAS 22192+6302 (in core E) and IRAS 22202+6317 (no core). These negative results, however, are based on the observation of only one spectrum (12″ resolution) with contamination from the OFF position, so we cannot rule out the existence of molecular outflows at low velocities.

4. RESULTS FROM THE NH_3 OBSERVATIONS

The cores identified in CS(1–0) were further studied in ammonia with an angular resolution of 40″. We present their NH_3(1, 1) integrated intensity maps in Figure 4. Core A had previously been studied in ammonia by Ungerechts, Walmsley, & Winnewisser (1986), and we observed only its central position for calibration purposes. Verdes-Montenegro et al. (1989) mapped core B in ammonia at lower resolution; our results are in good agreement with theirs.

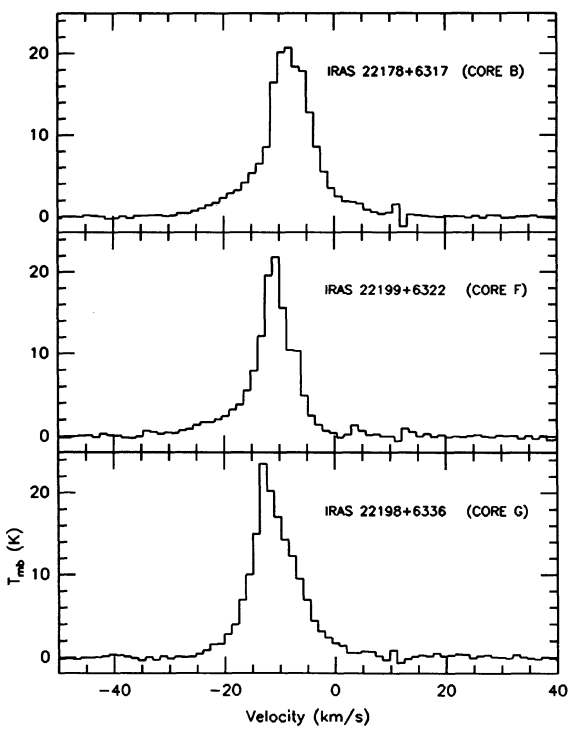

FIG. 3.—CO(2–1) spectra toward the three *IRAS* sources where high-velocity gas was detected.

4.1. *Physical Conditions of Cores*

We analyzed the ammonia data with the method described in Bachiller, Guilloteau, & Kahane (1987). From the (1, 1) profiles, it is possible to estimate the optical depth by comparing the intensities in the five groups of hyperfine components. We assumed that the excitation temperature, T_{ex}, is the same for all the hyperfine components, and that it is uniform along the line of sight. We made nonlinear least-square fits to the observed spectra with the following independent parameters: (1) the opacity of the main group of hyperfine components, τ_m, (2) the central line velocity, (3) the intrinsic line width, and (4) the quantity $X = \phi\tau_m(T_{ex} - T_{bg})$, where ϕ is the beam filling factor.

The (2, 2) emission was considerably weaker than the (1, 1) emission, and it was detected only toward the peak positions of some maps. As only the main hyperfine component was discerned, a single Gaussian was fitted.

From the fits to the (1, 1) and (2, 2) profiles, it is possible to obtain the NH_3 column densities in the (1, 1) and (2, 2) levels and the rotation temperature T_{12}. The gas kinetic temperature can be determined by solving the statistical equilibrium equations; these equations are simplified by considering only the three lower rotational levels of NH_3 (see, for example, Walmsley & Ungerechts 1983; Danby et al. 1988). Once the kinetic temperature is known, it is possible to derive the total NH_3 column densities (see Bachiller et al. 1987). Table 3 summarizes the (1, 1) and (2, 2) observational parameters, as well as the (1, 1) opacities and NH_3 column densities, for the peak positions in the cores.

The excitation temperatures given in Table 3 were calculated from the X parameter and the opacity, assuming a filling factor of 1. The volume densities can then be estimated from T_{ex} and T_{bg} by assuming that the (1, 1) doublet behaves as a two-level system. For the cores in L1204, these estimates for T_{ex} and n are not very accurate because the cores are small and the filling factor can be smaller than 1 (see Fig. 4). An alternative possibility is to assume that the transition is thermalized and to derive the beam filling factor from the value of X. This assumption, however, produced excessively small values of ϕ. Thus, it appears that we are in an intermediate situation with $\phi < 1$, $T_{ex} < T_K$. We have preferred to consider the approximation $\phi = 1$ and to look at the T_{ex} values as rough estimates. Typical lower limits to n are (1–2) $\times 10^4$ cm^{-3}, kinetic temperatures at the emission maxima are in the range 15–20 K, and the ammonia column densities range from 2×10^{14} to 7×10^{14} cm^{-2}. Our results for the S140-IRS position in core A are in good agreement with those derived by Ungerechts et al. (1986).

4.2. *Core Dynamics: Velocity Shifts*

In five cores the ammonia lines suffer sudden velocity changes of $\sim$0.5–0.8 km s^{-1} that seem to divide the cores into two velocity regimes. In Figure 5 we present, for each core, two

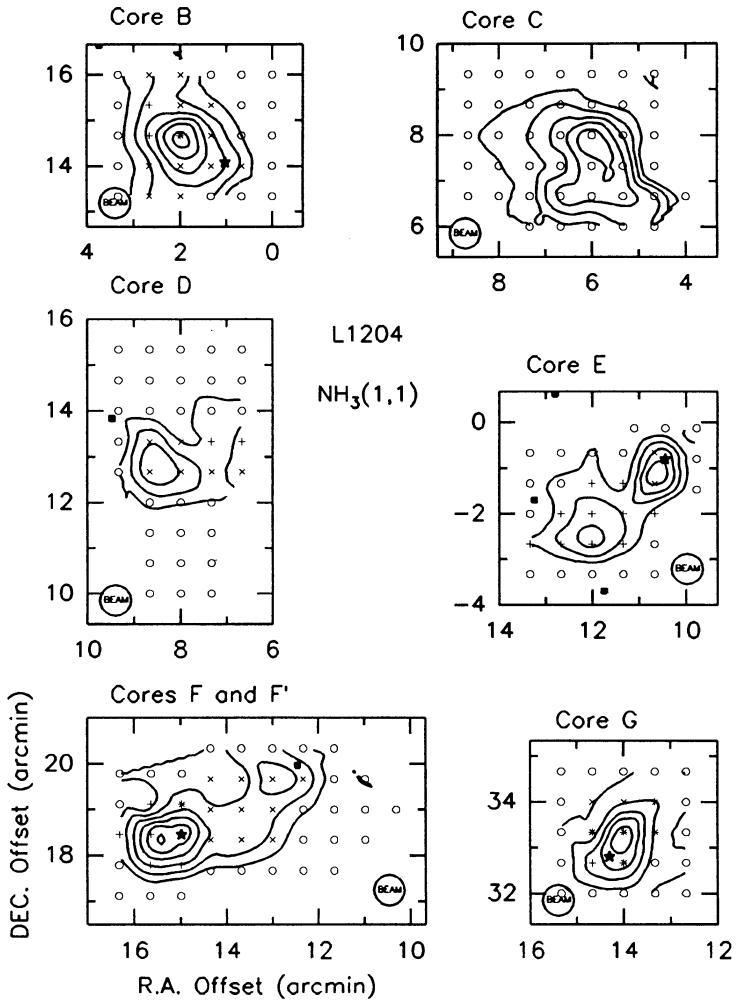

FIG. 4.—Maps of the $NH_3(1, 1)$ integrated emission in the cores of L1204. Crosses (×) indicate positions with red emission. Plus signs (+) indicate positions with blue emission. The superposition of a cross and a plus sign indicates a mixture of red and blue emission. Circles indicate observed positions where the emission was too weak to allow a spectrum classification or, in core C, all the positions, because only one velocity component was found. Filled stars and squares indicate *IRAS* point sources as in Fig. 1*a*. Position offsets are with respect to the (0, 0) position of Fig. 1. First contour and contour step are 0.6 K km s^{-1} (core B, *top left*), 1 and 0.3 K km s^{-1} (core C, *top right*), 0.65 and 0.25 K km s^{-1} (core D, *middle left*), 0.5 and 0.25 K km s^{-1} (core E, *middle right*), 0.5 K km s^{-1} (cores F and F', *bottom left*), and 0.5 K km s^{-1} (core G, *bottom right*).

spectra from positions separated by 80″ (0.35 pc) showing the red and blue components.

The geometry of the velocity shifts is not well resolved by our observations because of the compact ammonia emission. Only in core F is the emission extended enough that the velocity field can be studied with detail. The position-velocity diagram along an east-west line (Fig. 6) shows that the ammonia line keeps a constant velocity before and after the shift, which occurs in a region unresolved by our 40″ beam. In the other cores, the emission is not extended enough to allow meaningful position-velocity diagrams. The velocity fields are better discerned if each spectrum is classified as red or blue and its position is represented on a map. This is done in Figure 4, where the blue spectra are indicated by plus signs (+) and the

TABLE 3

PARAMETERS FROM NH_3 OBSERVATIONS

Core	Offset[a] ($\Delta\alpha$, $\Delta\delta$)	$T_B(1, 1)$ (K)	$T_B(2, 2)$ (K)	V_{LSR} (km s^{-1})	ΔV (km s^{-1})	$\tau_m(1, 1)$	$T_{ex}(1, 1)$ (K)	T_K (K)	$N(NH_3)/10^{14}$ [b] (cm^{-1})
B	(2, 14.7)	2.8	0.9	−8.74	1.0	1.2	7	15	5.7
C	(6, 8)	1.3	0.5	−7.24	1.6	0.2	10	20	2.0
D	(8.7, 12.7)	1.3	...	−6.23	0.6	1.0	5	...	2.0
E	(10.7, −1.3)	0.8	...	−8.51	0.9	2.3	4	...	5.0
F	(15.9, 18.5)	1.5	...	−10.80	1.1	0.7	6	...	3.0
G	(14, 33.3)	1.6	0.3	−11.08	1.3	1.3	5	12	6.8

[a] Offset in arcminutes with respect to the central position of the maps in Fig. 1.

[b] For the positions where T_K is not measured, we assumed $T_{12} = 15$ K ($T_K = 15.5$ K) in the calculation of the NH_3 column densities.

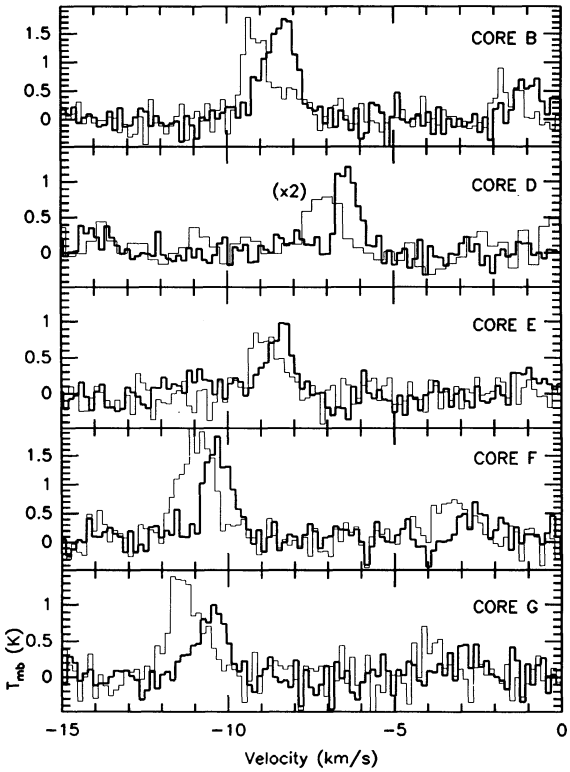

FIG. 5.—Velocity shifts observed in the $NH_3(1, 1)$ line toward the five cores containing *IRAS* sources. Thick line corresponds to the red component and thin line to the blue component. The position of the spectra for the red and blue components are, respectively: core B, (1.3, 14) and (2.7, 14.7); core D, (8.6, 12.7) and (7.3, 13.3) (blue spectrum multiplied by 2 and smoothed for easier comparison); core E, (10.7, −0.7) and (11.3, −2); core F, (14.3, 18.5) and (15.7, 18.5); core G, (14, 34) and (14.7, 32.7). All offsets are referred to the S140-IRS position (see Fig. 1).

red spectra by crosses (×). Some positions have wider spectra, as if resulting from the overlap of the blue and red regimes, and they are indicated by the superposition of a cross and a plus sign.

The velocity shifts are not the result of a partial absorption of the ammonia lines, because they are also seen, if the emission is strong enough, in the satellite components of $NH_3(1, 1)$ and in the main component of $NH_3(2, 2)$, which have much smaller opacities. The shifts represent real gradients in the velocity of the emitting gas. We have estimated these gradients by selecting nearby positions and dividing their velocity difference by their spatial separation, assuming a distance of 910 pc. These gradients, presented in Table 4, range from 1 to 3 km s^{-1} pc^{-1}, and are much larger than those measured in the large-scale maps of L1204, indicating that the velocity shifts are not part of a global velocity pattern, but are an effect localized in the cores.

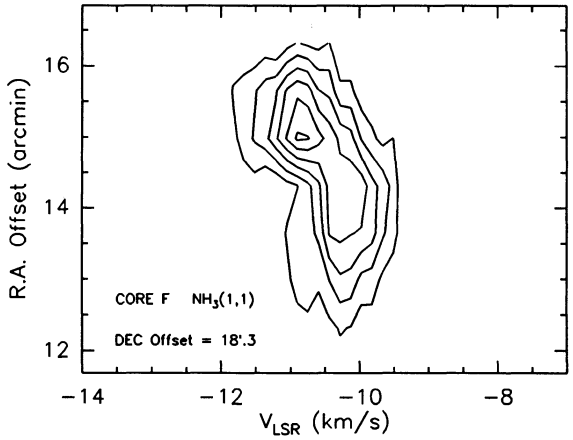

FIG. 6.—Position velocity diagram along an east-west line in core F. Declination offset is 18'.3. Contours are 0.3, 0.6, ... K.

The detection rate of velocity shifts is high (five out of six cores present some evidence for them), and although the number of cores is still very small, some trends seem to appear: (1) The shifts seem to be associated with *IRAS* sources, as the only core with no evidence for a velocity shift (core C) is the only one without a nearby *IRAS* source; (2) The velocity shifts seem to coincide with the ammonia emission maximum, even if it is offset from the *IRAS* source; (3) One velocity component seems to dominate, being more extended than the other.

5. DISCUSSION

5.1. *Comparison between* CS *and* NH_3 *Data*

The CS and NH_3 observations were done with very different resolutions, and the 2′ beam used to observe CS(1–0) samples an area 9 times larger than that sampled by the 40″ beam used for ammonia. In order to make a proper comparison between the two emissions, the NH_3 data were degraded to simulate the result of 2′ beam observations. Because of the smaller coverage in ammonia, we will limit our comparison to the spectra of the central position of each core.

The emission velocities of the two molecules (obtained from fits to the spectra) agree within 0.2 km s^{-1}, indicating a close relation of the gases traced by each species. The line widths, however, do not show such a good agreement, and in three cores (B, C, and D), the CS(1–0) lines are wider than the $NH_3(1, 1)$ lines by a factor between 1.5 and 2. In E, F, and G, on the other hand, the CS and NH_3 linewidths are consistent. This dichotomy is due to the narrow CS lines measured in the latter cores and not to a change in the ammonia lines, which have similar widths in all the cores.

Differences in line width between NH_3 and CS are common. Zhou et al. (1989) have reported, from a survey of low-mass molecular cloud cores, that the CS lines are wider than the

TABLE 4

AMMONIA VELOCITY SHIFTS

Core	Red Position	Red V_{LSR} (km s^{-1})	Blue Position	Blue V_{LSR} (km s^{-1})	Shift (km s^{-1})	Gradient (km s^{-1} pc^{-1})
B	(1′.3, 14′.0)	−8.43	(2′.7, 14′.7)	−9.19	0.76	1.9
D	(8.7, 12.7)	−6.35	(7.3, 13.3)	−7.16	0.81	2.1
E	(10.7, −0.7)	−8.43	(11.3, −2.0)	−8.90	0.47	1.2
F	(14.3, 18.3)	−10.15	(15.0, 18.3)	−10.76	0.61	3.3
G	(14.0, 34.0)	−10.50	(14.7, 32.7)	−11.32	0.82	2.1

NH_3 ones by typically a factor 2. They argue that optical depth effects do not explain these differences, and that some other process, like chemical differentiation, could be their cause. This difference raises the question whether NH_3 is tracing the same gas as CS, and, in our case, whether the kinematics seen in NH_3 represent the kinematics of the bulk of the gas. Although our CS(1–0) data alone cannot prove that both kinematics are similar, the good agreement between the emission velocities, better than the size of the shifts, argues in favor of it. Also, preliminary high-resolution CS observations of cores B, F, and G (Tafalla & Bachiller 1992) show velocity shifts analogous to the ammonia ones. We therefore believe the velocity structure seen in ammonia represents the real velocity structure of the gas in the cores.

5.2. *Origin of Ammonia Velocity Shifts*

The simplest explanation for the ammonia velocity shifts, without involving any gas acceleration, would be the random superposition of different clouds along the line of sight. In fact, the large-scale CS maps show that L1204 contains three clouds that sometimes overlap. The difference in their velocities, however (~ 2 km s^{-1}), their extension, and their spatial distribution, cannot explain that the velocity shifts are always smaller than 1 km s^{-1} and occur only at scales comparable to the core size. Small-scale superposition of different cores is also unlikely, because the suddenness of the velocity changes would imply a geometry where independent cores superpose so one begins where the other ends. The velocity shifts, therefore, indicate real structure in the kinematics of the dense gas.

Velocity structure in dense cores has been previously observed by different authors. Sometimes it has been interpreted as the result of core rotation (e.g., Kaifu et al. 1984, for L1551), others, as the result of interaction with the outflows from the embedded YSOs (Moriarty-Schieven et al. 1987, for the same object), and others, as the combination of both (Menten & Walmsley 1985, also for L1551). In particular, the Cep A ammonia data of Güsten, Chini, & Neckel (1984) show velocity features similar to those of the cores in L1204, and the position-velocity diagram across Cep A strongly resembles that of core F (Fig. 6). These authors interpret their observations as providing evidence for a rotating circumstellar disk in Cep A.

In principle, rotation and outflow could be distinguished through observations. Solid-body rotation, for example, should produce a systematic velocity pattern, with the velocity difference between two positions increasing proportional to their distance. Outflow acceleration, on the other hand, as a more local effect, should be restricted to the vicinity of the YSOs and be correlated with the high-velocity CO emission. In practice, however, the distinction is not easy, due to the lack of resolution, and to the complicated outflow geometries and velocity patterns of the dense gas.

If the velocity shifts in L1204 are due to rotation, the velocity gradients we have measured would correspond to angular velocities of $3\text{–}9 \times 10^{-14}$ s^{-1}. These values are similar to those found by Arquilla & Goldsmith (1986) for a sample of dark clouds. Their survey, however, was biased toward clouds with known or suspected rotation, and was sensitive mostly to low-density gas because of the use of CO transitions. A more recent study by Goodman et al. (1992) shows that velocity gradients in dense cores are common. By fitting solid-body rotation curves to the ammonia velocity fields of a large sample of cores, they derive velocity gradients that range from 0.3 to 4 km s^{-1} pc^{-1}, with a typical value of 1 km s^{-1} pc^{-1}. The values we obtain for the cores in L1204 are within that range, but they lie at its high end, as four cores present gradients of ~ 2 km s^{-1} pc^{-1} or more. These systematically larger values could be due to our different method of measuring the gradients, to an overestimate of the distance for the cloud, or to a faster rotation of the cores in L1204. The geometries we find, however, and, in particular, the "flat rotation curve" of core F (Fig. 6), indicate that patterns more complicated than solid-body rotation should be considered.

The other interpretation of the velocity shifts, that they are the result of the acceleration of the dense gas by bipolar outflows, is also possible. In fact, all the cores with velocity shifts seem to be associated with *IRAS* sources that, in three cases, are driving molecular outflows. (The situation in cores D and E is more uncertain, see § 3.3.) Unfortunately, a proper comparison between the outflows and the velocity shifts is not possible with the present observations. The only outflow with known geometry is the one in core B (also known as S140N), mapped by Fukui et al. (1986). Their map shows an outflow well centered on the *IRAS* source and with east-west bipolarity, the east emission blue and the west emission red. Our NH_3 spectra present a shift in the same sense as the CO outflow, but centered on the NH_3 emission maximum, which is offset 70″ from the *IRAS* object. In core F, where most of the gas is at red velocities and the ammonia lines shift to the blue near the *IRAS* source, the outflow is mostly blue. This is shown by our CO(2–1) spectrum in Figure 3 and by Fukui's (1989) table of outflows (where it is classified as "blue"), and it suggests a possible outflow-shift correlation. Although compelling, these results are still very incomplete and high-resolution mapping of the outflows and the dense gas is necessary.

If the outflows produce the velocity shifts, they should have enough energy and momentum to accelerate the dense gas. The properties of the outflows are not known, so we cannot compare them directly to those of the accelerated dense gas. If we assume that the outflow energy and momentum are correlated with the luminosity of the infrared source, as found by Bally & Lada (1983), we can obtain rough estimates of the energy and momentum supply rate. The uncertainty, however, is very large, as can be seen from the scatter in the plots of Bally & Lada (see also Lada 1985). By also assuming outflow ages of 3×10^4 yr (a typical value from Levreault's 1988 survey), we obtain energies and momenta comparable to those needed to produce the ammonia shifts. The outflows, in principle, seem to have enough energy and momentum to cause the ammonia shifts.

Although our data do not have the resolution to clearly distinguish between rotation and acceleration by outflows as the cause of the velocity structure, the presence of molecular outflows inside the cores indicates some disturbance of the dense gas. If the outflow material is swept up gas from the cloud (Snell 1987) it seems natural to imagine that the dense gas around the YSO has been perturbed and accelerated. We therefore believe that, at least partially, the ammonia velocity structure is due to the interaction with the outflows. The assessment of the relative importance of rotation awaits higher resolution observations.

6. CONCLUSIONS AND SUMMARY

We have presented CS and NH_3 observations of the L1204/S140 complex. The complex consists of three clouds with different velocities, each of them containing extended emission and several discrete maxima that we identify with dense cores.

Most cores are sites of recent star formation, as they are associated with *IRAS* sources having spectral distributions characteristic of YSOs. Some also present high-velocity emission in their CO spectra, clear evidence of molecular outflow. At the small scales, the cores with YSOs have a complicated kinematics. The ammonia lines present shifts in velocity ($\sim$0.5–0.8 km s^{-1}) and, in some cases, two different velocity components seem to exist inside the core. The most likely causes for these velocity shifts are rotation of the cores or the acceleration of the dense gas by the bipolar outflows from the embedded YSOs.

We thank the staff of the observatories at Yebes, Effelsberg, and Pico Veleta for their generous support during the observations. We also thank J. Montalbán for interesting discussions on the CS(1–0) data, Matthew Richter for his careful reading of the manuscript and the referee, Neal Evans, for useful comments. This research was partially supported by the Spanish CICYT (project number PB88-0453). MT was partially supported by a Spanish MEC/Fulbright grant and by the NSF grant AST 88–15406 to the Radio Astronomy Laboratory, which are gratefully acknowledged.

REFERENCES

Arquilla, R., & Goldsmith, P. F. 1986, ApJ, 303, 356
Bachiller, R., Guilloteau, S., & Kahane, C. 1987, A&A, 173, 324
Bally, J., & Lada, C. J. 1983, ApJ, 265, 824
Blair, G. N., Evans, II, N. J., Vanden Bout, P. A., & Peters, III, W. L. 1978, ApJ, 219, 896
Blair, G. N., & Vanden Bout, P. A. 1974, BAAS, 6, 452
Castor, J. I. 1970, MNRAS, 149, 111
Crampton, D., & Fisher, W. A. 1974, Pub. Dom. Astrophys. Obs., 14, 283
Danby, G., Flower, D. R., Valiron, P., Schilke, P., & Walmsley, C. M. 1988, MNRAS, 235, 229
Evans, II, N. J., Mundy, L. G., Kutner, M. L., & DePoy, D. L. 1989, ApJ, 346, 212
Fukui, Y. 1989, in ESO Workshop on Low-Mass Star Formation and Pre–Main-Sequence Objects, ed. B. Reipurth (Munich: ESO), 95
Fukui, Y., Sugitani, K., Takaba, H., Iwata, T., Mizuno, A., Ogawa, H., & Kawabata, K. 1986, ApJ, 311, L85
Goodman, A. A., Benson, P. J., Fuller, G. A., & Myers, P. C. 1993, ApJ, submitted
Güsten, R., Chini, R., & Neckel, T. 1984, A&A, 138, 205
IRAS Point Source Catalog, Version 2. 1988, Joint *IRAS* Science Working Group (Washington, DC: US GPO)
Kaifu, N., et al. 1984, A&A, 134, 7
Kutner, M. L., & Ulich, B. L. 1981, ApJ, 250, 341
Lada, C. J. 1985, ARA&A, 23, 267
Lada, C. J. 1987, in IAU Symp. 115, Star Forming Regions, ed. M. Peimbert & J. Jugaku (Dordrecht: Reidel), 1
Lester, D. F., Harvey, P. M., Joy, M., & Ellis, H. B. Jr. 1986, ApJ, 309, 80
Leung, C. M., Herbst, E., & Huebner, W. F. 1984, ApJS, 56, 231
Levreault, R. M. 1988, ApJS, 67, 283
MacLaren, I., Richardson, K. M., & Wolfendale, A. W. 1988, ApJ, 333, 821
Menten, K. M., & Walmsley, C. M. 1985, A&A, 146, 369
Moriarty-Schieven, G. H., Snell, R. L., Strom, S. E., & Grasdalen, G. L. 1987, ApJ, 317, L95
Scoville, N. Z., & Solomon, P. M. 1974, ApJ, 187, L67
Snell, R. L. 1987, in IAU Symp. 115, Star Forming Regions, ed. M. Peimbert & J. Jugaku (Dordrecht: Reidel), 213
Snell, R. L., Mundy, L. G., Goldsmith, P. F., Evans, II, N. J., & Erickson, N. R. 1984, ApJ, 276, 625
Sugitani, K., & Fukui, Y. 1987, in IAU Symp. 115, Star Forming Regions, ed. M. Peimbert & J. Jugaku (Dordrecht: Reidel), 75 (SF)
Tafalla, M., & Bachiller, R. 1992, in preparation
Ungerechts, H., Walmsley, C. M., & Winnewisser, G. 1986, A&A, 157, 207
Verdes-Montenegro, L., Torrelles, J. M., Rodriguez, L. F., Anglada, G., López, R., Estalella, R., Cantó, J., & Ho, P. T. P. 1989, ApJ, 346, 193
Walmsley, C. M., & Ungerechts, H. 1983, A&A, 122, 164
Zhou, S., Wu, Y., Evans, II, N. J., Fuller, G. A., & Myers, P. C. 1989, ApJ, 346, 168